RSC Advances

ROYAL SOCIETY OF CHEMISTRY

www.rsc.org/advances

Configurable Plasmonic Substrates from Heat-driven Imprint-Transferred Ag Nanopatterns for Enhanced Photoluminescence

Yeon-Ho Jung[1,2], Sang-Keun Sung[1], Kyung-Min Lee[3], Srivathsava Surabhi[3], Jun-Ho Jeong[1], Eung-sug Lee[1], Jun-Hyuk Choi[1*], Jong-Ryul Jeong[3*]

[1]Nanomechanical Systems Research Division, Korea Institute of Machinery and Materials, Yuseong-gu, Daejeon 305-343, South Korea

[2]Department of Nano-Mechatronics, University of Science and Technology, Yuseong-gu, Daejeon 305-350, South Korea

[3]Department of Materials Science and Engineering and Graduate School of Energy Science and Technology, Chungnam National University, Daejeon 305-764, South Korea

*To whom correspondence should be addressed. E-mail: jrjeong@cnu.ac.kr, junhyuk@kimm.re.kr

Abstract

Despite substantial progress in metal nanopatterning, fabricating ultra-large-area plasmonic substrate with well-defined and well-controlled nanopatterned arrays remains a major technological challenge. Here, we describe a novel facile technology (*i.e.*, configurable metal nanoimprint transfer based on geometric reconfiguration during thermal annealing) to fabricate ultra-large-area tunable plasmonic substrates. The simultaneous transfer and imprint of the metal layers from the patterned mold surface results in metal nanopatterns embedded in a partially cured photoresist, the shape of which can be modified systematically by optimized heat treatments. The plasmonic properties of the metal nanopattern array could be precisely tuned through the heat-driven shape reconfiguration of metal patterns. The shape transformation is leading to sharp and blue-shifted extinction spectra and unusual strong excitation of the transverse mode of metal nanopatterns. Coarse tuning of the plasmon resonance wavelength is achieved by varying the diameter of the nanopatterned features, and fine tuning is accomplished by reconfiguring the geometry of the nanopatterned features *via* thermal annealing. Only three master patterns are required to cover the wavelength range 535–837 nm. By applying the plasmon substrates to photoluminescence (PL) measurement, an enhancement in the green photoluminescence (PL) intensity of a factor more than 9.4 is achieved due to the improved matching between the wavelengths for PL emission and plasmon resonance. The fabrication strategy described here enables us to achieve various plasmonic properties using a single master pattern, which provides both tailorable plasmonic properties and remarkable process flexibility.

Keywords: Tunable plasmonic substrate, Metal nanopatterning, Selective nanoimprint, Tunable photonics.

1. Introduction

Metallic nanostructures, a particularly attractive area of research due to their unique plasmonic properties, have numerous applications in various optoelectronic devices and optical sensing devices. Several studies have reported that the efficiency of various optoelectronic devices can be dramatically improved using resonant plasmonic enhancement by coupling the electromagnetic field using a properly designed metallic nanostructure.[1–10] Such metallic nanostructures are often referred to as metallic photonic crystals or plasmonic nanostructures. The plasmonic properties of these nanostructures depend critically on the geometry and choice of materials,[10–13] and techniques to fabricate large-area metallic nanostructures are required, which has been a limiting factor in realizing plasmonic devices with the designed functions.

For example, plasmonic nanostructures for plasmonic luminescence have been experimentally achieved using randomly distributed silver (Ag) and gold (Au) nanoparticles,[4–7] which is easier than using well-controlled arrays; however, the process is clearly less controllable, and correspondingly, we can expect the plasmonic enhancement to be less substantial. To address this problem, the large-area plasmonic substrates with well-defined nanopattern array have been fabricated using nanoimprint lithography (NIL) together with advanced metal liftoff processes.[8–10,14–16] Metal corrugations have been achieved either by depositing a metal film onto a pre-patterned surface[17–21] or by using metal direct nanoimprinting.[22,23] However, the metal lift-off process and the completely covered metal corrugation naturally suffers from the difficulties associated with the multi-step processes and reduced transmittance. In addition, many corresponding master designs should be separately prepared for each required plasmonic peak wavelength and spectra profile. This would lead to

costly fabrication if various applications are in pursuit, especially with features sizes that are less than 100 nm (which corresponds to wavelengths shorter than green light) over a large area. In this respect, many existing fabrication strategies as referred above lack process reliability, accessibility, and further cost competitiveness because of numerous process steps involved and the limited tunability.

Here, we describe a novel method for fabrication of configurable large-area plasmonic substrate by heat-driven direct metal imprint transfer. Tuning of the plasmon resonance wavelength was achieved by reconfiguring the transferred metal nanopatterns using thermal annealing. In this manner, even single mold pattern can provide plasmonic absorption peaks at various wavelengths, which provides plasmonic properties tunability and reduces the cost for multiple applications.

The process parameters, including the temperature, thickness of the deposited metal layer, and mold pattern, were varied to investigate the effects on the transmittance associated with the plasmon resonance and the subsequent photoluminescence (PL) enhancement.

2. Experiments

Fig. 1 shows a schematic diagram of the heat-driven direct metal imprint transfer procedure. The metal used, silver in this work, was evaporated on a replicated nanoimprint mold as shown in Fig. 1a. An ultraviolet (UV)-curable adhesive resist was coated on the transparent substrate and partially pre-cured under UV exposure to increase its viscosity (Fig. 1b), facilitating mold release without affecting the integrity of the imprinted patterns. The master patterns were replicated to produce pillars on a custom polyurethane acrylate UV-curable resin on a polyethylene terephthalate (PET) film, which was used as the nanoimprint

mold. The mold resin consisted of tri-propylene glycol diacrylate (Aldrich) and tri-methylol-propane triacrylate (Aldrich) as a monomer, with 4 wt% 2,2-dimethoxy-2-phenylacetophenone (Aldrich) as the photoinitiator and 1–4 wt% Rad 2200N (TEGO Chemi Service) as the releasing agent. The imprint mold was surface-treated with FOTS (Trichloro(1H,1H,2H,2H-perfluoro-octyl)silane, Aldrich) to provide hydrophobicity so that the metal film can be easily transferred in the afterward. Ag was then evaporated onto the mold pattern surfaces to form a layer with a 20-60 nm using *e*-beam evaporator prior to the imprint transfer. . By imprinting onto the pre-cured adhesive resist (see Fig. 1c), selective transfer of Ag onto the top surface of the patterns could be achieved, with an optimized pre-cure UV exposure and imprint pressure.

Epoxy-based UV curable resist (NOA61, Norland Inc.) was used to selectively adhere the Ag layer on the top surface of the mold pattern. UV exposure with a pulse energy of 9 mJ was used to partially cure the resist (about 50% of its complete cure energy) to realize a half-embedded profile of the imprint-transferred Ag patterns. Optimizing this UV exposure was important as excessive pre-curing of the resist would not allow the Ag to be transferred because of the diminished stickiness, even with an increased imprint pressure; however, insufficient UV exposure made releasing the mold difficult. Considering this criterion, The imprint pressure was optimized to 0.5 bar. A subsequent UV exposure was used to completely cure the resist and allow mold release (Fig. 1d). The samples were exposed to UV energy of 18 mJ, while applying the required imprint pressure to completely cure the adhesive polymer. Thereafter, the samples were annealed at an elevated temperature to reconfigure the transferred Ag structures (Fig. 1e). The temperature of this anneal was varied in steps of 50°C up to 250°C.

The patterned plasmonic substrates were used to investigate plasmonic enhancement to the photoluminescence (PL). The green PL materials $Ir(ppy)_3$ ([Tris[2-phenylpyridinato-C^2,*N*]iridium(III)] from EM Index Co., Korea) were dissolved in chlorobenzene, doped with PMMA, spin-coated onto the oxide–coated sample surfaces, and then baked on a hot plate at 80°C for 20 min. The PL spectra of the $Ir(ppy)_3$–PMMA films exhibited an excitation peak at 355 nm and an emission peak at 510 nm. PL spectra were measured in FluoroLog Spectrofluorometer (Horiba Jobin Yvon, USA), where the samples were mounted for the back-side excitation using a Xe lamp in the UV-visible range at an angle of < 45°.

Three dimensional finite-difference time-domain (FDTD) simulations were performed to theoretically model the plasmonic properties of the Ag nanopatterns. A grid size of 0.1 nm was used. The Drude model is used to describe the complex permittivity of Ag nanopatterns and the index of the glass substrate and NOA layer is measured by spectroscopic ellipsometry.

3. Results and Discussion

Selective transfer of only Ag on the top pattern surface of the mold resulted in the Ag being embedded in the imprinted patterns, as identified in Fig. 2(a). In order to reconfigure the metal nanopatterns transferred into the layer of NOA, subsequent thermal annealing was carried out. Fig. 2b and 2c shows the variation of the morphology of the nanopatterned Ag features, which had an initial diameter of d = 150 nm and thickness of t = 20 nm, as the annealing temperature was increased up to 250°C. The as-transferred Ag pillars were cylindrical and were transformed into ellipsoids at temperatures above 200°C, with an increase in the maximum thickness and a reduction in the diameter. Figure 2d shows the change in geometry following annealing at various temperatures schematically. The change in

diameter was estimated based on the SEM images; for Ag pillars with d = 150 nm and t = 20 nm, we find that the diameter decreased by about 40% following annealing at 250ºC; 211 nm when Ag imprint-transferred becomes to 130nm after thermal annealing. The changes in geometry at such relatively temperatures low can be ascribed to melting-point depression of metallic nanostructures due to thermodynamic size effects. We also attempted to observe the changes in the geometry of thicker and larger nanopatterned Ag features. Figure 3a presents SEM images of Ag pillars with d = 150 nm and t = 60 nm, and Fig. 3(b) shows SEM images for nanopatterns with d = 265 nm and t = 40 nm, both of which were annealed at 250°C. The features clearly exhibited ellipsoidal forms, with an increase in the maximum thickness. In particular, the thinner pillars resulted in features that were almost spherical, and narrow trenches in the photoresist were visible around the imprinted holes (Fig. 3b).

These temperature-dependent changes in the geometry are expected to affect the plasmonic properties of the Ag nanopatterns because the polarizability and plasmon resonance of the nanostructures depend on both the size and shape of the structure. The effects of annealing at different temperatures were investigated for Ag pillars with d = 200 nm and d = 150 nm nanopatterns, and with t = 40 nm. Figure 4 shows a clear blue-shift of the plasmon resonance peaks with increasing annealing temperature. For the patterns with a diameter of d = 200 nm, the plasmon resonance of the as-prepared pattern occurred at 699 nm and shifted to 621 nm following annealing at 250ºC (Fig. 4a). For the patterns with a diameter of d = 150 nm, the plasmon resonance of the as-prepared pattern was at 606 nm and shifted to 535 nm following annealing at 250ºC (Fig. 4b), representing a shift in the plasmon resonance peak of up to 78 nm (d = 200 nm) and 71 nm (d = 150 nm). Note that the second extinction peak of the transmittance around 400 nm became larger when the annealing

temperature increased to 250°C.

Figure 5 shows a summary of wavelength tunability of the plasmonic substrates. Coarse tuning of the plasmon resonance wavelength was achieved by changing the diameter of the nanopatterns from 150 nm to 265 nm, whereas fine tuning was accomplished by reconfiguring the shape of the nanopatterns. Note that only three given master patterns were required to cover almost whole wavelength range 535–837 nm excluding niche gap approximately from 700 nm to 750 nm. It suggests the optimized annealing conditions can provide the significant range of corresponding plasmon resonance wavelengths for single master pattern.

To elucidate the mechanism for the shifts in the plasmon resonance peak and the appearance of the additional plasmonic peak, three-dimensional FDTD calculations were carried out to model the UV-vis spectra of the Ag nanopatterns. In this simulation, we assumed that the Ag nanopatterns changed from cylinders (with d = 200 nm and t = 40 nm) to ellipsoids (Fig. 6a) and the depth of the imprinted hole in which the Ag nanopatterns are embedded is fixed. . In this simulation, The Ag nanopatterns were excited using a linearly polarized plane wave propagating in the k = -z direction (Fig. 6b). The boundary conditions in x and y directions were set to periodic boundary conditions and the top and bottom boundaries (±z direction) are terminated with a perfectly matched layer (PML). To simplify the calculation, the glass substrate is assumed fairly thick with no transmission by using a PML under the glass substrate.

As expected, decreasing the major axes of the ellipsoids a and b, and increasing the of minor axis c (corresponding to an increase in the annealing temperature), led to a sharper and a blueshift of the extinction spectra of the Ag nanopatterns (Fig. 6c). The blue-shifted

extinction spectra should be regarded to result from a decrease in the in-plane length of the Ag features. Figures 6d and 6e show the electric field intensity distribution at $\lambda_1 = 656$ nm and $\lambda_2 = 586$ nm; the primary extinction peaks are associated with a longitudinal plasmon mode. Figure 6f shows the electric field intensity distribution at $\lambda_3 = 385$ nm. In contrast to the electric field distributions shown in Figs. 6d and 6e, which are related to the longitudinal plasmon mode, a transverse plasmon mode in the z direction can be clearly seen. This transverse mode is considerably less polarizable and therefore less sensitive to changes in the geometry; however, excitation of the transverse mode can be obtained by reconfiguring the Ag nanopatterns. In general, such transverse plasmon resonance occurs at a higher frequency than the longitudinal mode and thus shorter wavelength. Therefore, creating a plasmon resonance at wavelengths <500 nm using a patterned array of 150-nm-diameter features is a significant advantage of the technique described here. Without the reconfiguration of the pillars following thermal annealing, creating a plasmon resonance at wavelengths <500 nm would require master patterning at a scale less of than 100 nm, which is technically challenging, especially to achieve with a viable cost and over a large area (100×100 mm^2 in this work).

The reconfigurable plasmonic substrates described here have potential applications in optoelectronic devices, including light-emitting applications,[4–10] solar cells,[14] and sensors.[15,16] To investigate the applicability of the reconfigurable plasmonic substrates to such optoelectronic applications, we carried out PL measurements. The green photoluminescent material $Ir(ppy)_3$ was used, and we attempted to match the excitation and emission wavelengths to the plasmon resonances. The excitation wavelength of $Ir(ppy)_3$ was $\lambda_{ex} = 355$ nm, and the emission wavelength was $\lambda_{em} = 510$ nm. Prior to the deposition of the

photoluminescent layer, a 20-nm-thick oxide layer was deposited as a spacer to exclude quenching effects due to nonradiative decay in a close proximity with the metal.[24] Figure 7a shows the PL intensity for the $Ir(ppy)_3$ deposited on a nanopatterned substrate formed of Ag pillars with d = 150 nm following annealing at various temperatures. By incorporating the Ag nanopatterns, we obtained an enhancement of the PL of a factor of 5.7 compared to that of the reference sample, the NOA film without the patterned Ag features. By annealing the Ag nanopatterned array, the PL intensity was further increased, providing an enhancement of up to a factor of 9.4.

In general, the PL enhancement σ_{PL} is a function of absorption cross section at the excitation frequency $\sigma_a(\omega_{ex})$ and the radiative efficiency $\eta_{rad}(\omega_{em})$, and can be expressed as follows: [25]

$$\sigma_{PL}(\omega_{ex},\omega_{em})=\sigma_a(\omega_{ex})\cdot\eta_{rad}(\omega_{em}) \qquad (1)$$

Since the incident electromagnetic energy is proportional to the electric field enhancement, one can expect the increased absorption because of the surface plasmon mode excitation as shown in the inset of Fig. 6g and 6h. It clearly shows the electric field enhancement at the surface of the Ag nanopatterns. Due to the large interdot distance, no electric field enhancement can be seen between the nanopillars. However, the electric field enhancement at the excitation and wavelength ($\lambda=\lambda_{ex}$) is relative weak compared to the electric field enhancement at the surface plasmon resonance wavelength ($\lambda=\lambda_{SP}$). Therefore, we cannot significant enhancement of the absorption cross section due to the enhanced electric field intensity. In addition to the enhanced absorption cross section mediated by enhanced electric field intensity around the Ag nanopatterns, a significant enhancement of the PL is expected when the plasmon resonance wavelength is close to the PL emission wavelength due to the

outcoupling of the surface plasmon mode into the radiative mode. As shown in Figs. 4 and 5, thermal annealing resulted in a blueshift of the plasmon resonance wavelength, which makes it closer to λ_{ex}; this may be expected to increase the emission efficiency. Figure 7b shows the PL enhancement factor as a function of the wavelength difference between the excitation wavelength λ_{ex} and the longitudinal plasmon resonance wavelength λ_{SP}, which shows that the PL enhancement was proportional to the difference in wavelength and suggests that resonance matching was the major enhancement mechanism.

The enhancement in the PL was also investigated for nanopatterned features with various diameters. Figure 8 shows the PL intensity and corresponding enhancement factors for nanopatterns with d = 150, 200, and 265 nm. The enhancement in the PL intensity was similar for all diameter Ag features. Note that the PL intensity was enhanced even with a large difference between λ_{ex} and λ_{SP}; *e.g.*, we find an enhancement of a factor of 5.7 for $\lambda_{ex} - \lambda_{SP}$ = 403 nm. These enhancements can be explained by considering the electric field intensity owing to the transverse mode in the reconfigured nanopatterns. Therefore, we can conclude that the transverse mode that exists following the reconfiguration of the nanopillars allows the resonant energy in the plasmon mode to be more effectively out-coupled, which facilitates PL emission and modifies the radiative decay rate due to the intense electric field. [25-26] The PL enhancements achieved here are significantly greater than previously reported results.[11, 14, 26–28] PL enhancements were in the range of five-folds when randomly distributed gold nanoparticles were applied [11, 14], about 100 % ~ 300 % applying silver nanoparticle distributions transformed thermally [26, 27], and 280% PL enhancement of SiC nanocrystal by proximal silver nanoparticles [28]. Distinguished PL enhancements in this work are attributed to better-matched resonance condition in controlled structure array, which enables the resonance

coupling to be focused and intensified at the designed particular wavelength.

Additionally note that our reconfigurable large-area plasmonic substrates represent a wafer-scale fabrication and the technique is preferable to randomly distributed nanoparticles in terms of reproducibility. Additionally, the wavelength tunability provides major potential advantages and multipurpose flexibility.

4. Conclusion

In this work, we investigated a simple metal nanopatterning technique based on direct metal imprint transfer consisting of selective transfer of a metal layer only on the top surface of an imprinted mold pattern and the following geometric transformation of the metal patterns using thermal annealing. Sharp blue-shifted extinction spectra due to the nanopatterned Ag features were observed following the thermal anneal, which are due to a decrease in the effective diameter of the Ag pillars. Strong excitation of the transverse mode was obtained following the geometric reconfiguration of the Ag nanopillars. The plasmon resonance wavelength was tuned coarsely by changing the diameter of the nanopillars from 150 nm to 265 nm and more finely tuned by reconfiguring the geometry of the features. Only three master patterns were required used to tune over the wavelength range 535−837 nm. The PL intensity from $Ir(ppy)_3$ deposited on the patterned substrates was investigated, and we found a significant enhancement following the reconfiguration of the patterns. By optimizing the annealing temperature, an increase in the PL intensity of a factor of 9.4 was observed. The enhancement data should be superior than previously reported, probably due to more effective resonance coupling from better-matched resonance condition in controlled structure array.

The fabrication technique described here can be used to realize various plasmonic properties using a single master pattern by varying annealing temperature. In comparison with previous works based on metal lift-off or metal corrugation, the major points of the present process can be summarized as the followings; (1) to confine the metal aggregation into well-controlled hole array, (2) to combine the metal transfer (for selective metal deposition) with nanoimprint (for well-controlled hole array). Therefore, controlled plasmonic structural arrays can be fabricated at a wafer scale, and the plasmon resonance can be tuned easily, providing major potential advantages of multipurpose flexible fabrication with low costs.

Acknowledgments

This research was supported by grants from the Basic Science Research Program (2011-0028585, 2014M3C1A3052569, 2013R1A2A2A01067144, 2013R1A4A1069528), funded by the National Research Foundation of Korea (NRF) under the Ministry of Education, Science and Technology. It was also funded by Institute Project (SC1100) of KIMM (Korea Institute of Machinery & Materials).

References

1 K. Saxena, V. K. Jain and D. S. Mehta, *Opt. Mater*., 2009, **32,** 221.

2 J. Yao, A. P. Le, S. K. Gray, J. S. Moore, J. A. Rogers and R. G. Nuzzo, *Adv. Mater*., 2010, **22,** 1102.

3 N. C. Lindquist, P. Nagpal, K. M. McPeak, D. J. Norris and S. H. Oh, *Rep. Prog. Phys*., 2012, **75,** 036501.

4 C. Y. Wu, C. L. He, H. M. Lee, H. Y. Chen and S. Gwo, *J. Phys. Chem. C*, 2010, **114,** 12987.

5 Y. Xiao, J. P. Yang, P. P. Cheng, J. J. Zhu, Z. Q. Xu, Y. H. Deng, S. T. Lee and Y. Q. Li, *Appl. Phys. Lett*. 2012, **100,** 013308.

6 A. Fujiki, T. Uemura, N. Zettsu, M. Akai-Kasaya, A. Saito and Y. Kuwahara, Appl. Phys. Lett, 2010, **96**, 043307.

7 A. Kumar, R. Srivastava, D. S. Mehta and M. N. Kamalasanan, Org. Electron, 2010, **13**, 1750.

8 K. H. Cho, J. Y. Kim, D. G. Choi, K. J. Lee, J. H. Choi and K. C. Choi, Opt. Lett, 2012, **37**, 761.

9 Y. Wang, T. Yang, M. T. Tuominen and M. Achermann, Phys. Rev. Lett, 2009, **102**:163001.

10 G. F. Walsh and L. D. Negro, Nanoletters, 2013, **13**, 786.

11 B. Zeng, Y. Gao and F. J. Bartoli, Scientific Rep. 2013, **3**, 2840.

12 X. J. Liu, G. Y. Si, E. S. P. Leong, B. Wang, A. J. Danner, X. C. Yuan and J. H. Teng, App. Phys. A, 2012, **107**, 49.

13 K. Kumar, H. Duan, R. S. Hegde, S. C. W. Koh, J. N. Wei and J. K. W. Yang, Nat. Nanotechnol, 2012, **7**, 557.

14 K. Nakaji, H. Li, T. Kiba, M. Igarashi, S. Samukawa and A. Murayama, Nanoscale Res. Lett, 2012, **7**, 629.

15 V. E. Ferry, J. N. Munday and H. A. Atwater, Adv. Mater. 2010, **22**, 4794.

16 Y. Jin, Adv. Mater. 2012, **24**, 5153.

17 J. Maria, T. Truong, J. Yao, T. W. Lee, R. G. Nuzzo, S. Leyffer, S. K. Gray and J. A. Rogers, J. Phys. Chem. C, 2009, **113**, 10493-10499.

18 X. L. Zhang, J. Feng, J. F. Song, X. B. Li and H. B. Sun, Appl. Phys. Lett, 2011, **36**, 3915.

19 J. Feng and T. Okamoto, Opt. Exp, 2005, **30**, 2302.

20 V. Reboud, N. Kehagias, T. Kehoe, G. Leveque, C. Mavidis, M. Kafesaki and C. M. Sotomayer Torres, Microelectron. Eng, 2010, **87**, 1367.

21 Y. Bai, J. Feng, Y. F. Liu, J. F. Song, J. Simonen, Y. Jin, Q. D. Chen, J. Zi, and H. B. Sun, Org. Electron, 2011, **12**, 1927.

22 S. S. Kim, Y. Xuan, V. P. Drachev, L. T. Varghese, L. Fan, M. Qi and K. J. Webb, Opt. Exp. 2013, **21**, 15081.

23 C. C. Liang, M. Y. Liao, W. Y. Chen, T. C. Cheng, W. H. Chan and C. H. Lin, Opt. Exp. 2011, **19**, 4768.

24 K. Ray, H. Szmacinski, J. Enderlien and J. R. Lakowicz, Appl. Phys. Lett, 2007, **90**, 251116.

25 G. Sun, J. B. Khurgin and R. A. Soref, *Appl. Phys. Lett*. 2009, **94,** 101103.

26 C. Y. Cho, M. K. Kwon, S. J. Lee, S. H. Han, J. W. Kang, S. E. Kang, D. Y. Lee and S. J. Park, Nanotechnology 2010, **21**, 205201.

27 M. K. Kwon, J. Y. Kim, B. H. Kim, I. K. Park and C. Y. Cho, Adv. Mater. 2008, **20**, 1253.

28 N. Zhang, D. J. Dai, and J. Y. Fan, Appl. Surf. Sci. 2012, **258**,10140.

Figure captions

Fig. 1 Schematic diagram illustrating the direct metal nanoimprinting and subsequent change in geometry following thermal annealing.

Fig. 2 SEM images of the Ag nanopatterns annealed at (a) room temperature, (b) 200°C, and (c) 250°C. (d) Schematic diagram of the geometry transformation following annealing at various temperatures. The insets show tilted and cross-sectional SEM images.

Fig. 3 SEM images of Ag nanopatterns with (a) d = 150 nm and t = 60 nm, and (b) d = 265 nm and t = 40 nm, both annealed at 250°C. The insets show tilted and cross-sectional SEM images.

Fig. 4 The UV-vis transmittance spectra of the Ag nanopatterns following annealing temperature at various temperatures. (a) With d = 200 nm and (b) with d = 150 nm.

Fig. 5 The resonance wavelength as a function of the annealing temperature for various diameter nanopatterned Ag features.

Fig. 6 Schematic diagrams showing (a) the geometric parameters and (b) the geometry used in the simulations. (c) The calculated transmittance spectra with various geometric parameters. (d, e) Pseudocolor plots showing the electric field intensity distributions for (d) λ 656 nm, (e) λ = 586 nm, and (f) λ = 385 nm. (g, h) The in plane electric field intensity distributions of a=b=95 nm nanopatterns for (g) λ = 355 nm and (h) λ = 656 nm.

Fig. 7 (a) PL intensity spectra with various annealing temperatures, and (b) the enhancement in the PL factor as a function of the difference between the excitation wavelength λ_{ex} and the

longitudinal plasmon resonance wavelength λ_{SP}. The enhancement of the PL was calculated by normalizing the PL intensity at the peak wavelength to that of the reference sample (*i.e.*, the cured resist with no Ag nanopatterned features).

Fig. 8 (a) PL intensity spectra with various diameter Ag nanopillars, all annealed at 250ºC, and (b) the enhancement in the PL factor as a function of the difference between the excitation wavelength λ_{ex} and the longitudinal plasmon resonance wavelength λ_{SP}. The enhancement of the PL was calculated by normalizing the PL intensity at the peak wavelength to that of the reference sample (*i.e.*, the cured resist with no Ag nanopatterned features).

Figure 1

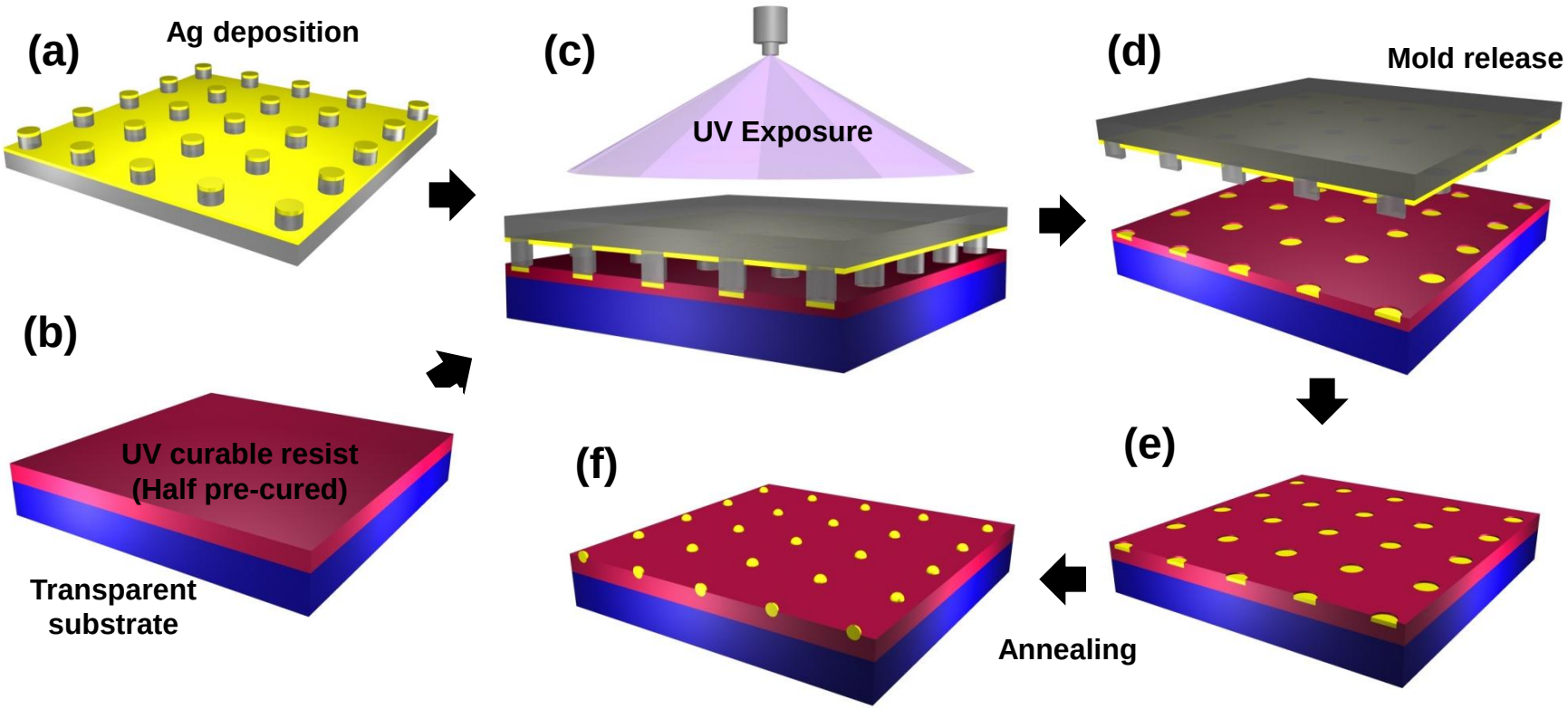

Figure 2

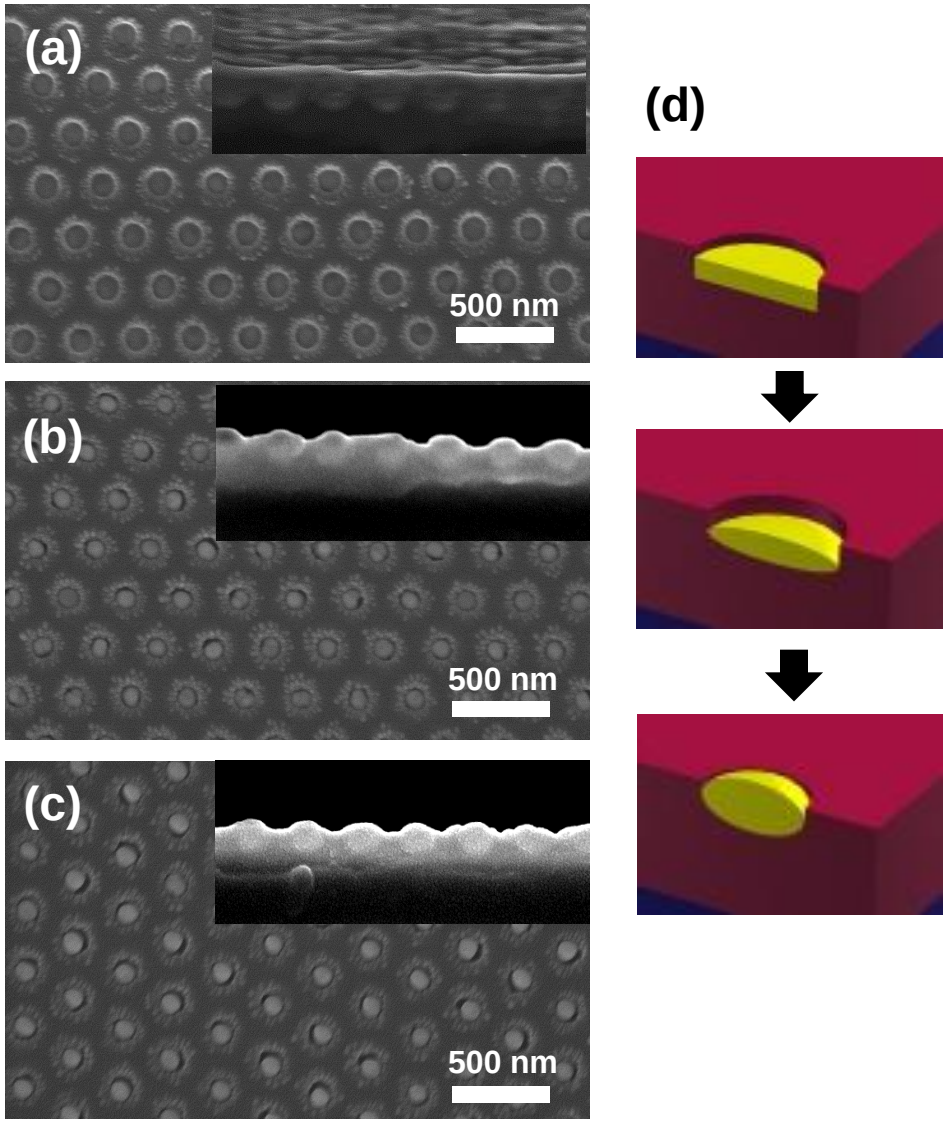

Figure 3

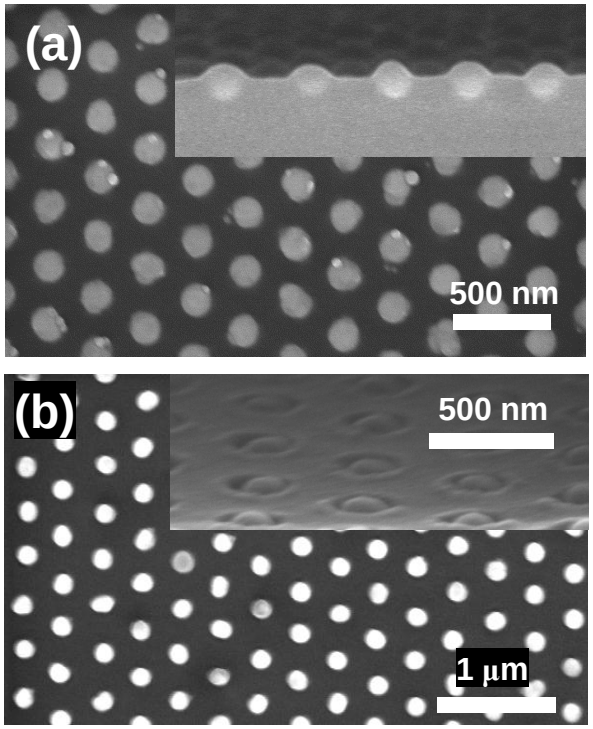

Figure 4

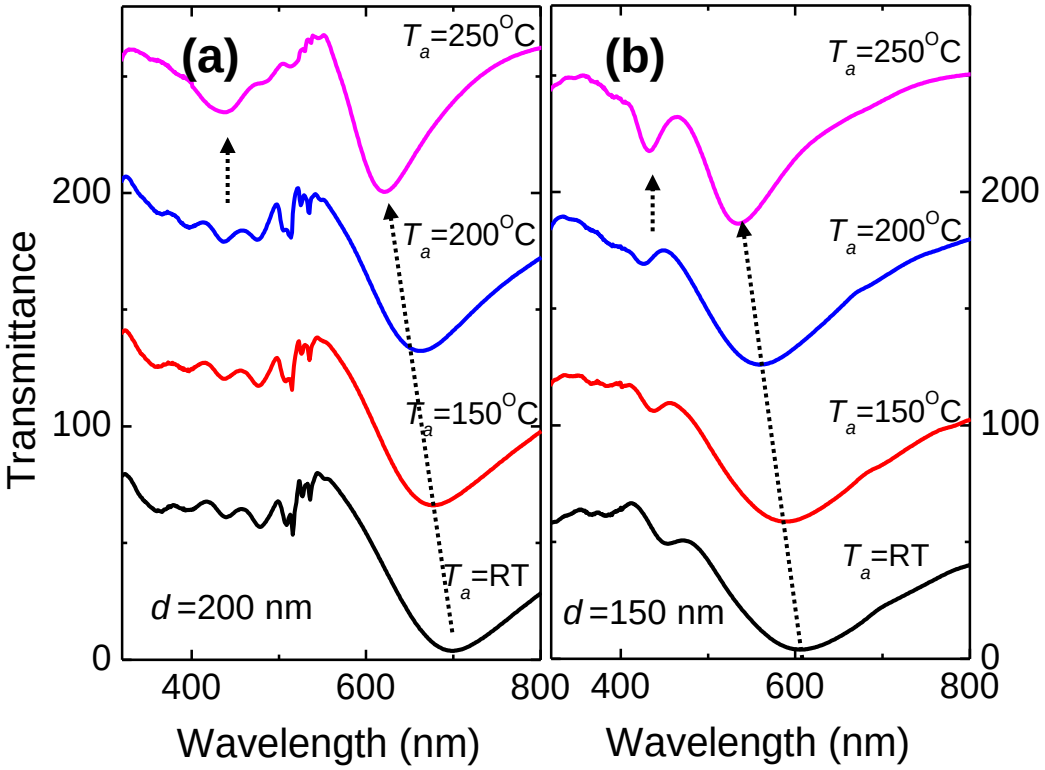

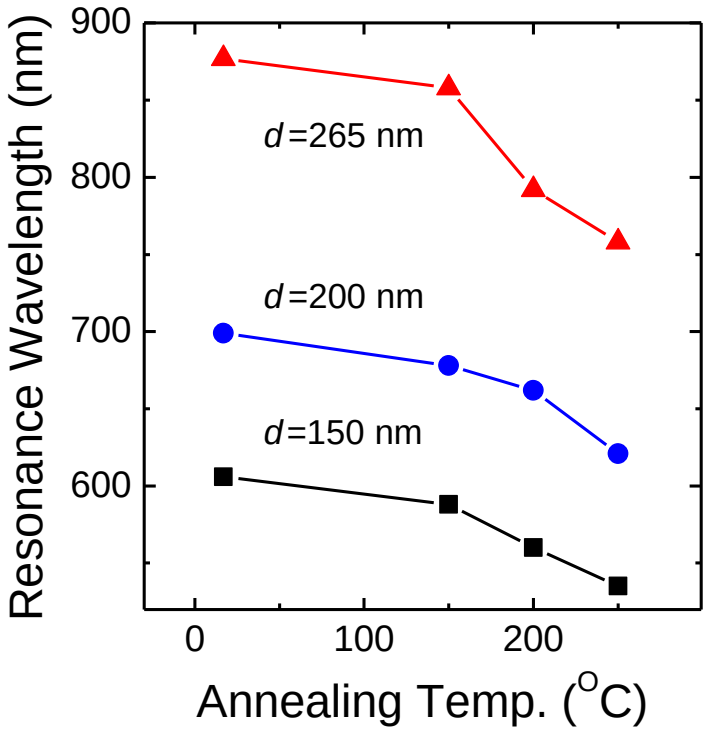

Figure 6

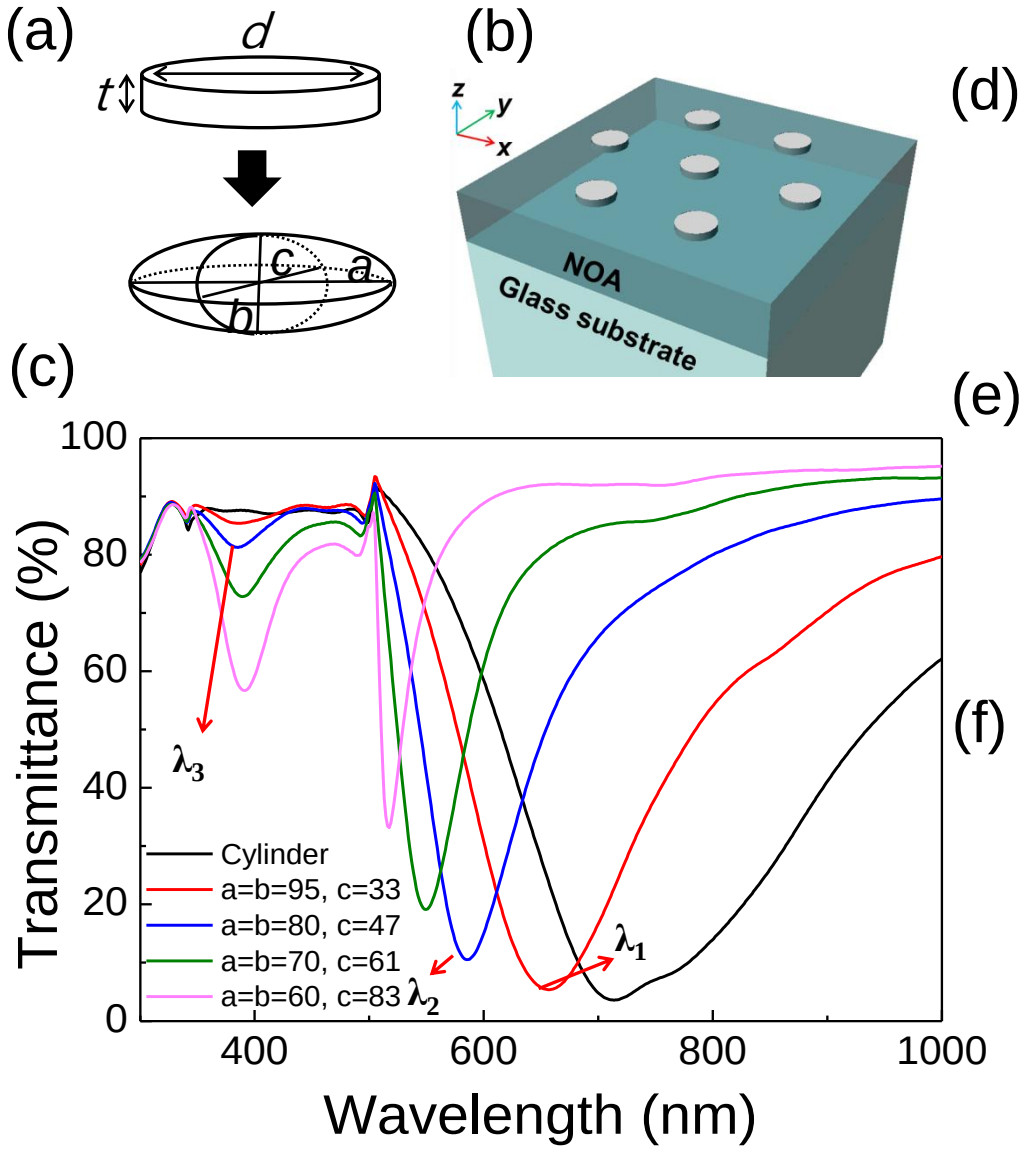

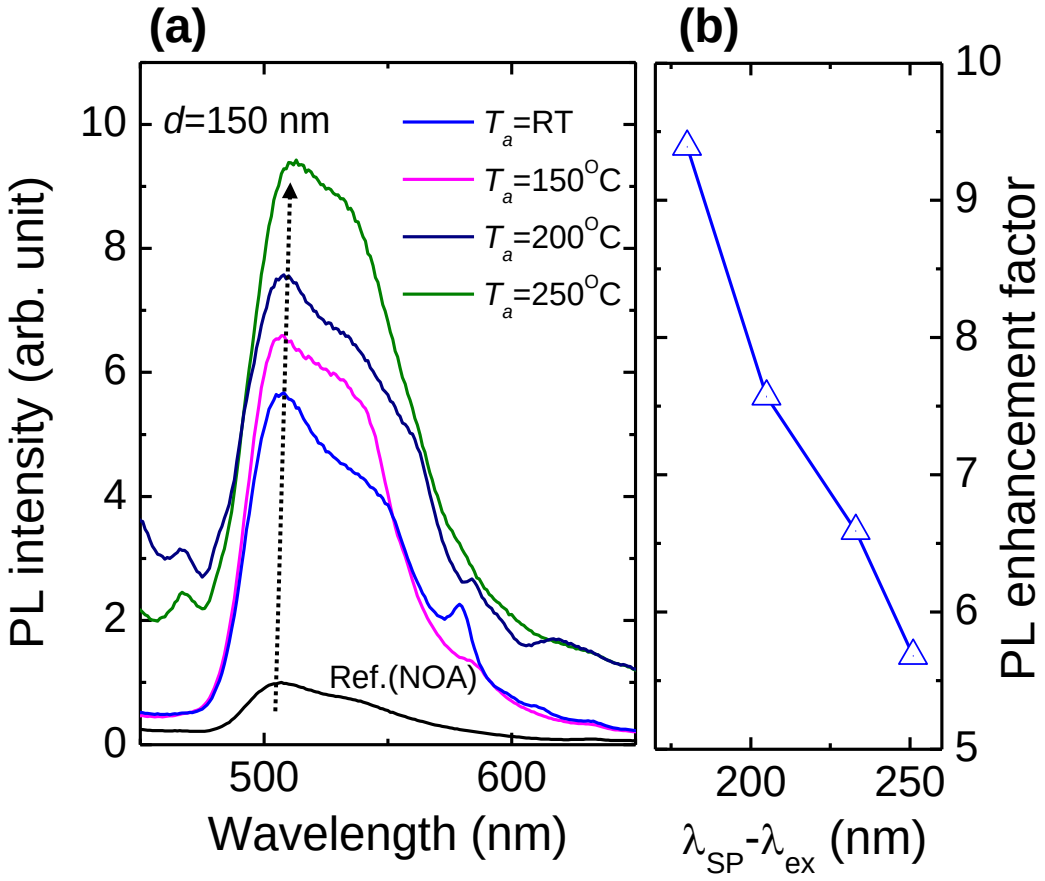

Figure 8